HHS Public Access

Author manuscript

Med Image Comput Comput Assist Interv. Author manuscript; available in PMC 2016 January 01.

Published in final edited form as:

Med Image Comput Comput Assist Interv. 2015 October ; 9351: 751–759. doi: 10.1007/978-3-319-24574-4_90.

Multi-scale Heat Kernel based Volumetric Morphology Signature

Gang Wang[1,2] and **Yalin Wang**[2,★]

[1]Ludong University, School of Information and Electrical Engineering, Yantai, China, 264025

[2]Arizona State University, School of Computing, Informatics, and Decision Systems Engineering, Tempe, AZ, USA, 878809

Abstract

Here we introduce a novel multi-scale heat kernel based regional shape statistical approach that may improve statistical power on the structural analysis. The mechanism of this analysis is driven by the graph spectrum and the heat kernel theory, to capture the volumetric geometry information in the constructed tetrahedral mesh. In order to capture profound volumetric changes, we first use the volumetric Laplace-Beltrami operator to determine the point pair correspondence between two boundary surfaces by computing the streamline in the tetrahedral mesh. Secondly, we propose a multi-scale volumetric morphology signature to describe the transition probability by random walk between the point pairs, which reflects the inherent geometric characteristics. Thirdly, a point distribution model is applied to reduce the dimensionality of the volumetric morphology signatures and generate the internal structure features. The multi-scale and physics based internal structure features may bring stronger statistical power than other traditional methods for volumetric morphology analysis. To validate our method, we apply support vector machine to classify synthetic data and brain MR images. In our experiments, the proposed work outperformed FreeSurfer thickness features in Alzheimer's disease patient and normal control subject classification analysis.

Keywords

Heat kernel; Volumetric Laplace-Beltrami operator; Point distribution model; Support vector machine

1 Introduction

In Alzheimer's disease (AD) research, several MRI-based measures of atrophy, including cortical thickness, hippocampal atrophy or ventricular enlargement, are closely correlated with changes in cognitive performance, supporting their validity as biomarkers of early AD identification. As we know, the MRI imaging measurement of medial temporal atrophy is not sufficiently accurate on its own to serve as an absolute diagnostic criterion for the clinical diagnosis of AD at the mild cognitive impairment (MCI) stage. A key research question is how to select the features which have a high discriminatory power. For example,

★This work was partially supported by the joint special fund of Shandong province Natural Science Fundation (ZR2013FL008), National Natural Science Foundation of China (61471185), National Health Institutes (R21 AG043760,U54EB020403) and National Science Foundation (DMS-1413417,IIS-1421165).

the cortical thickness was the popular feature which has been used to capture the difference between different clinical groups. Currently, there are two different computational paradigms on brain cortical thickness, with methods generally classified as either surface or voxel based [1, 2]. However, all measured distances are unitary distances between boundary points and they are unitary values that suggest only global trends and cannot capture topological variations (e.g. the regional information along the connecting curves is not considered). To address these difficulties, we introduce diffusion geometry methods to compute multi-scale intrinsic volumetric morphology signatures. Because the 2D shape analysis cannot offer the internal volumetric structure information within the solid volume such as brain grey matter. Based on some recent work [3,4] which studied volumetric heat kernel and the volumetric Laplace-Beltrami operator [5], here we propose a multi-scale heat kernel statistic to describe the transition probability by random walk between white-grey matter and CSF-grey matter boundary point pairs. With the tetrahedral mesh representation, our work may achieve subvoxel numerical accuracy. They provide quantitative measures of brain changes which are important for evaluating disease burden, progression and response to interventions.

In our work, a new set morphological descriptors is used to represent the volumetric structure information, which depends on heat transmission time and is somewhat influenced by the topological properties on the heat transmission path. Following that, a point distribution model (PDM) is applied to reduce the feature dimensionality to make classification feasible. With the support vector machine (SVM), we extract the most discriminative features that expose the brain abnormal changes. We also test the effectiveness of our framework in classification experiments.

A major innovation here is that our formulations make it possible for profoundly analyzing the internal structural information. The multi-scale and physics based geometric features may offer more statistical power on the topological change analysis in grey matter morphology as preclinical AD biomarkers.

2 Methods

Fig. 1 shows the pipeline of the volumetric morphology signature system.

2.1 Theoretical Background

The heat kernel diffusion on differentiable manifold M with Riemannian metric is governed by the heat equation:

$$\Delta_M f(x,t) = \frac{\partial f(x,t)}{\partial t} \quad (1)$$

where $f(x, t)$ is the heat distribution of the volume at the given time. Given an initial heat distribution F: $M \to \mathscr{R}$, let $H_t(F)$ denotes the heat distribution at time t, and $\lim_{t\to 0} H_t(F) = F$. $H(t)$ is called the *heat operator*. Both Δ_M and H_t share the same eigenfunctions, and if λ_i is an eigenvalue of Δ_M, then $e^{-\lambda_i t}$ is an eigenvalue of H_t corresponding to the same eigenfunction.

For any compact Riemannian manifold, there exists a function $l_t(x, y)$: $\mathbb{R}^+ \times M \times M \to \mathbb{R}$, satisfying the formula

$$H_t F(x) = \int_M l_t(x, y) F(y) dy \quad (2)$$

where dy is the volume form at $y \in M$. The minimum function $l_t(x, y)$ that satisfies Eq. 2 is called the *heat kernel* [6], and can be considered as the amount of heat that is transferred from x to y in time t given a unit heat source at x. In other words, $l_t(x, \cdot) = H_t(\delta_x)$ where δ_x is the Direc delta function at x: $\delta_x(z) = 0$ for any $z \neq x$ and $\int_M \delta_x(z) = 1$.

According to the theory of the spectral analysis, for compact M, the heat kernel has the following eigen-decomposition heat diffusion distance:

$$l_t(x, y) = \sum_{i=0}^{\infty} e^{-\lambda_i t} \phi_i(x) \phi_i(y) \quad (3)$$

where λ_i and φ_i are the i^{th} eigenvalue and eigenfunction of the Laplace-Beltrami operator, respectively. The heat kernel $l_t(x, y)$ can be interpreted as the transition density function of the Brownian motion on the manifold.

2.2 Discrete Multi-Scale Volumetric Morphology Signature

On volumetric structure represented by a tetrahedral mesh, we can estimate the boundary point pairs (x and y) based on the heat propogation, e.g. [5]. Then we can compute the eigenfunctions and eigenvalues of L_p and then estimate the heat diffusion distance $l_t(x, y)$ by evaluating Eqn. 3. We define the evaluation of $l_t(x, y)$ between surface point pairs, x and y, with varying time t, as the *volumetric morphology signature (VMS)*. To establish measurements on the unified template for statistical analysis, the weighted spherical harmonic representation [7] is applied to build surface correspondence between the different surfaces.

In order to reveal the internal structure features in a way that best explains the variance in the *VMS*, we apply a point distribution model(PDM) [8] to extract the most informative features. Given a group of N tetrahedral meshes, we apply the eigenanalysis of the covariance matrix Σ of the *VMS* as follows:

$$\sum = \frac{1}{N-1} \sum_{i=1}^{N} (\mathbf{T}_i - \overline{\mathbf{T}})(\mathbf{T}_i - \overline{\mathbf{T}})^T \quad (4)$$
$$\sum P = DP$$

where $\mathbf{T}_i$ is the *VMS* of the ith tetrahedral mesh and $\overline{\mathbf{T}}$ is the mean *VMS* of N objects. The columns of P hold eigenvectors, and the diagonal matrix D holds eigenvalues of Σ. The eigenvectors in P can be ordered according to respective eigenvalues, which are proportional to the variance explained by each eigenvector. The first few eigenvectors (with greatest eigenvalues) often explain most of variance in the *VMS* data. Now any volumetric morphology signature $\mathbf{T}_i$ can be obtained using

$$\mathbf{T}_i = \overline{\mathbf{T}} + P v_i \quad (5)$$

where v_i is a vector containing the principal components which are called the *internal structure features*. It can be used to represent the principal internal structure information of the individual tetrahedral mesh in a new basis of the deformation models.

2.3 Internal Structure Feature Selection

Generally speaking, the additional features are theoretically helpful to improve the classifier performance. However, in practice, each additional feature adds a parameter to the classifier model which needs to be estimated, and misestimations that result from the less informative features can actually degrade performance. This is a form of overfitting. So there is a need to order the features from more information to less information. This tactics can improve the classification accuracy. We adopt a *t*-test on each feature and obtain a *p*-value associated with the statistical group difference. Thus, a lower *p*-value implies a more significant feature. In the following experiments, we will test the classification accuracies according to two different feature orderings.

3 Experimental Results

3.1 Synthetic Data Results

We conduct classification experimental studies on a synthetic data set. Fig. 2 shows two classes of 12 synthetic volumetric geometrical structures each, Class 1 shows the cylinders with a sphere hole and Class 2 shows the cylinders with a bump-sphere hole. First we compute the streamlines between the outer cylinder surface and the inner spherical surface and establish the measurements on the unified template [5]. Then the *VMS* can be obtained with Eqn. 3. Fig. 3(a) shows a volumetric tetrahedral mesh. The point pairs between the outer cylinder surface and the inner spherical surface is shown in (b). The *VMS* of this tetrahedral mesh is shown in (c), where the horizontal axis is *log*(*t*) and the vertical axis is the *VMS* value. Apply Eqn. 4 and Eqn. 5, we obtain the first 23 internal structure features of every object. Then the features have been scaled to [−1, +1] before the classification. The main advantage of scaling is to avoid attributes in greater numeric ranges dominating those in smaller numeric ranges. In (d), we validate the classification performance of the two different feature orderings using the leave-one-out cross-validation method based on the SVM classifier. One is the standard ordering according to the order of the eigenvalue of the covariance matrix Σ generated from the training data, which indicates the variance amount of every feature from large to small. The other is the *p*-value ordering of the features from the training data. From the results, we can see that the internal structure features based on *VMS* have the high discriminative power. The mean accuracy of *p*-value ordering is 93.7% and the mean accuracy of standard ordering is 84.8%. And the two orderings can achieve the best accuracy 100% with fewer features. Moreover, the main computation is the eigenanalysis of the covariance matrix. By using the Gram matrix for eigenanalysis, the computational time for PDM can be improved to $O(n_s^2 * n_l)$ time. n_s is the number of shapes and n_l is the resolution.

In addition, we illustrate the importance of the feature selection in the projection space. The direction vectors of the classification hyperplane from the training data can be calculated as $proj\_value = x_\delta^T * w$, where $x_\delta = x - \bar{x}$ indicates the heat diffusion distance difference between the individual and the average, *proj_value* is the projected value and *w* is the direction vectors of the classification hyperplane. Fig. 4 shows the classification results in the projection space, with the horizontal coordinate representing the projection data, and with the vertical coordinate used for the posterior probability of belonging to the particular class, (a) and (b) represent the training data distributions with the first *i*th feature number (i.e., 6 and 23) according to the *p*-value respectively. The symbol ◊ and ⋇ indicate the two classes. From the results we can see that the phenomenon of the data piling has become apparent with the increasing of the feature number, (c) and (d) are the test classification results based on the first 6 and 23 features respectively. And the symbol ◊ and ⋇ with red mark indicate the misclassification results. From the results in Fig. 4, when all the features are used in training data, is associated with low in-sample error rate and high out-of-sample error rate.

3.2 Application to Alzheimer's Disease

To validate whether *VMS* can improve the statistical power on brain MRI analysis, we apply it to study the volumetric differences associated with AD and Control groups on the Alzheimer's Disease Neuroimaging Initiative (ADNI) dataset [9]. We used the baseline T1-weighted images from 81 subjects consisting of 41 healthy controls (CTL) and 40 patients of Alzheimer's (AD). We apply FreeSurfer software [10] for skull stripping, tissue segmentation and surface reconstruction. Given the white matter and pial surfaces, the tetrahedral meshes are generated by an adaptively sized tetrahedral mesh modeling method [11]. After the boundary point pairs are estimated, we resample all the brain surface to a common template which contains 40962 sample points. This allows us to compare the *VMS* measurements across different cortical surfaces. Next we apply the point distribution model (PDM) to the *VMS* to obtain v_i which contains 80 internal structure features for every individual grey matter tetrahedral mesh. After the scaling process, all the features are scaled to the interval [−1, 1]. We apply a *t*-test on each feature and obtain a *p*-value associated with the test statistic. The results are shown in Fig. 5 (a). The second feature corresponds to $p = 2.29\times10^{-9}$, the third and fourth features correspond to $p = 1.34\times10^{-6}$ and $p = 1.51 \times 10^{-6}$ respectively, and for all the other features are above 1×10^{-3}. Based on the SVM classifier, we investigate the leave-one-out cross-validation accuracies using the first i features from the two different ordering of the features. The results are shown in Fig. 5 (b). From the results, we can see that the best accuracy (97.5%) can be achieved using few (e.g., 34) features based on the *p*-value ordering, while on the standard ordering, a good accuracy (88.9%) can be achieved using 42 features. Moreover, the mean cross-validation accuracy based on the *p*-value ordering is higher about (5%) than the standard ordering. From the Eqn. 5, the specific eigenvector has the weights to create the specific feature. Therefore, the most informative feature should correspond to the specific eigenvector with the most significant contribution for the group differences. We compute the L_2 norm of the specific eigenvector to obtain these weights according to the template surface. The weights from the first four eigenvectors are shown on the mean outer surface in Fig. 5. From (c) to (f), they are the computed weights from the first eigenvector to the fourth eigenvector. Large weights

correspond to locations with the most discrimination power. The weights are later color coded on the surface template point with the group difference *p*-map by different principal components. The values increase as the color goes from blue to yellow and to red. Because the second principal component has the smallest *p*-value, a significant difference exists in the medial temporal lobe region represented in Fig. 5 (d), supporting the fact that the medial temporal atrophy is the hallmark of AD disease.

3.3 Comparison with Freesurfer Thickness Feature

In this section, we compare the classification performance about the *VMS* and the thickness based on the Freesurfer method [10]. Here we apply the receiver operating characteristic (ROC) analysis to compare the discriminative power of the two analysis framework, which is created by plotting the true positive rate against the false positive rate at various threshold settings. After obtaining the thickness values on the unified template, we apply the PDM to the thickness to obtain v_i as the thickness feature. Through varying the threshold value which can determine the SVM classifier boundary, we can obtain the true positive rate, false positive rate and draw a ROC curve. The ROC curve is shown in Fig. 6 and the legend shows the two data set, the area under the ROC curve (AUROC) and the number of features used. Here we choose 42 *VMS* features and 55 cortical thickness features computed by Freesurfer to achieve the maximum AUROC according to the *p*-value feature selection scheme. And a completely random guess would give a diagonal line from the left bottom to the top right corners. The points above the diagonal represent good clas sification results (better than random), points below the line represent poor results (worse than random). From the result, we can see that the features of the *VMS* have the higher discriminative power than the cortical thickness.

A key reason for better classification is that *VMS* can not only compute geodesic distance between the point pairs, but it also compare the immediate neighboring volume changes along the geodesics. It may provide new insights to grey matter morphology study.

4 Conclusions and Future Work

Based on heat kernel analysis, we propose a novel multi-scale volumetric morphology signature. This has many applications in brain imaging research. Whether or not our new method provides a more relevant shape analysis power than those afforded by other criteria (folding, surface curvature, cortical thickness) requires careful validation for each application. Because different geometric properties produce different models, we plan to compare them in future for detecting subtle differences in brain structure for preclinical AD research.

References

1. Jones SE, Buchbinder BR, Aharon I. Three-dimensional mapping of cortical thickness using Laplace's equation. Hum Brain Mapp. Sep; 2000 11(1):12–32. [PubMed: 10997850]
2. Fischl B, Dale AM. Measuring the thickness of the human cerebral cortex from magnetic resonance images. Proc Natl Acad Sci USA. Sep; 2000 97(20):11050–11055. [PubMed: 10984517]
3. Raviv, D.; Bronstein, MM.; Bronstein, AM.; Kimmel, R. Proc Intl Workshop on 3D Object Retrieval (3DOR). ACM Multimedia; 2010. Volumetric heat kernel signatures; p. 39-44.

4. Castellani U, Mirtuono P, Murino V, Bellani M, Rambaldelli G, Tansella M, Brambilla P. A new shape diffusion descriptor for brain classification. MICCAI 2011, Lecture Notes in Computer Science. 2011; 6892:426–433.
5. Wang G, Zhang X, Su Q, Shi J, Caselli RJ, Wang Y. A novel cortical thickness estimation method based on volumetric Laplace-Beltrami operator and heat kernel. Med Image Anal. Feb; 2015 22(1): 1–20. [PubMed: 25700360]
6. Coifman RR, Lafon S, Lee AB, Maggioni M, Nadler B, Warner F, Zucker SW. Geometric diffusions as a tool for harmonic analysis and structure definition of data: multiscale methods. Proc Natl Acad Sci USA. May; 2005 102(21):7432–7437. [PubMed: 15899969]
7. Chung MK, Dalton KM, Shen Li, Evans AC, Davidson RJ. Weighted Fourier representation and its application to quantifying the amount of gray matter. IEEE Transactions on Medical Imaging. 2007; 26:566–581. [PubMed: 17427743]
8. Shen L, Ford J, Makedon F, Saykin A. A surface-based approach for classification of 3D neuroanatomic structures. Intelligent Data Analysis. 2004; 8:519–542.
9. Mueller SG, Weiner MW, Thal LJ, Petersen RC, Jack C, Jagust W, Trojanowski JQ, Toga AW, Beckett L. The Alzheimer's disease neuroimaging initiative. Neuroimaging Clin N Am. Nov; 2005 15(4):869–877. [PubMed: 16443497]
10. Fischl B, Sereno MI, Dale AM. Cortical surface-based analysis. II: Inflation, flattening, and a surface-based coordinate system. Neuroimage. Feb; 1999 9(2):195–207. [PubMed: 9931269]
11. Lederman C, Joshi A, Dinov I, Vese L, Toga A, Van Horn JD. The generation of tetrahedral mesh models for neuroanatomical MRI. Neuroimage. Mar; 2011 55(1):153–164. [PubMed: 21073968]

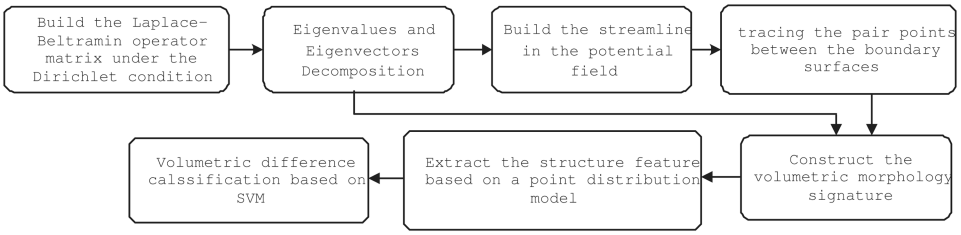

Fig. 1.
Pipeline of the volumetric morphology signature computation.

Fig. 2.
Two classes of synthetic volumetric geometrical structures.

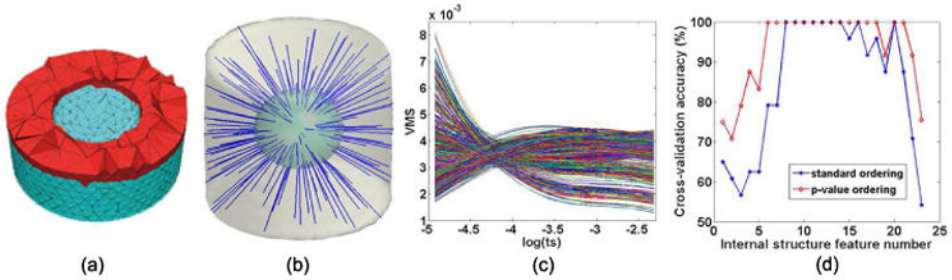

Fig. 3.

Illustration of streamlines, *VMS* and classification accuracies on the synthetic cylinder with inner spherical hole.

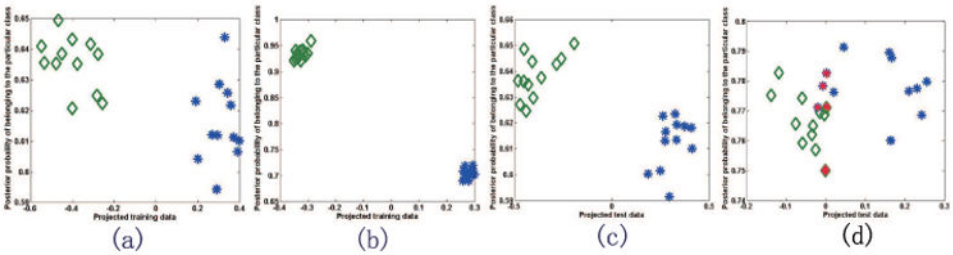

Fig. 4.

The training and test data classification results with the different feature number in the projection space.

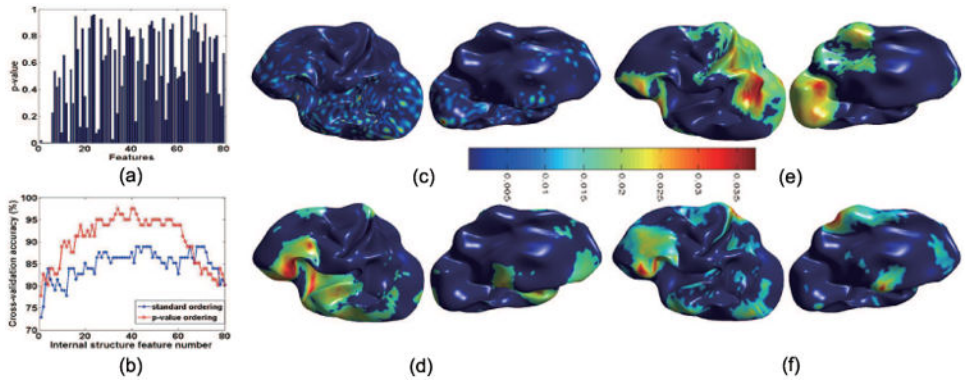

Fig. 5.

Illustration of the SVM classification accuracy and the contrubutions from the four eigenvectors color coded on the mean outersurface of AD and Control subjects.

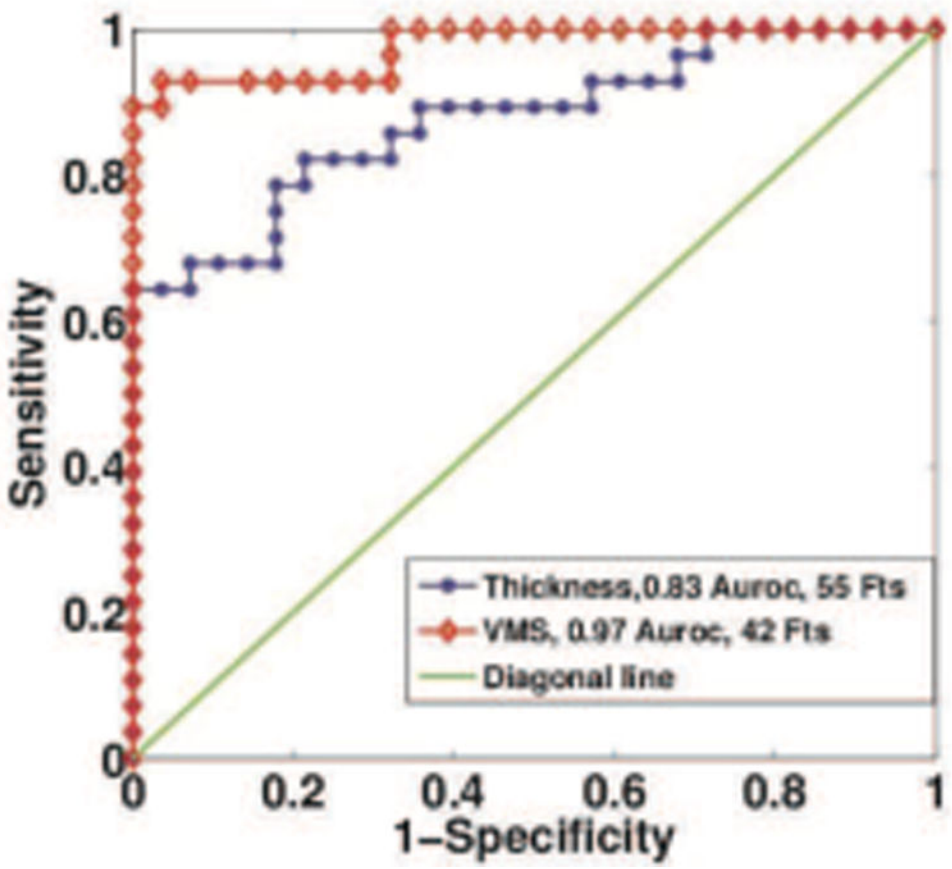

Fig. 6.
ROC analysis for comparison using *VMS* and thickness features.